Pore flow velocity measurement in filtration erosion enhanced with PIV technique

Yingyi Zhang,[1] Adnan Sufian,[2] and Alexander Scheuermann[3]

[1]Geotechnical Engineering Centre, School of Civil Engineering, The University of Queensland, St Lucia, Queensland, Australia; email: yingyi.zhang@uq.edu.au
Corresponding author.
[2]Geotechnical Engineering Centre, School of Civil Engineering, The University of Queensland, St Lucia, Queensland, Australia; email: a.sufian@uq.edu.au
[3]Geotechnical Engineering Centre, School of Civil Engineering, The University of Queensland, St Lucia, Queensland, Australia; email: a.scheuermann@uq.edu.au

ABSTRACT

This paper presents an experimental technique to observe particle-scale hydraulic behaviors in seepage-induced filtration erosion. Hydro-gel spheres were used as coarse filter particles, while a layer of fine glass spheres was placed beneath the layer of hydro-gel spheres as the finer cohesionless base particles in order to explore base-filter compatibility. An external upwards flow was applied through the sphere packing to trigger detachment of base particles. The Particle Image Velocimetry (PIV) technique enabled particle-scale observation and fluid velocity measurement. Water in the system was seeded with polyamide seeding particles (PSPs) to visualize particle displacement and water movement in the PIV system. This testing technique allowed observation within the pore space of the filter particle matrix, which was otherwise not accessible from imaging on external surfaces. Particle-scale hydraulic behaviors in filtration erosion can be quantitatively studied with this technique, enabling insights into the geometric and hydraulic criteria governing filtration erosion.

INTRODUCTION

Filtration erosion happens when finer soil particles (referred to as base particles) detach and migrate through the pore space of coarser soil particles (referred to as filter particles) due to high seepage flow rates. This phenomenon impacts soil stability significantly (Reddi et al. 2000; Tomlinson & Vaid 2000). Filtration erosion is found to happen in both natural soils and in engineered structures (Li & Fannin 2008), such as embankments and dams.

The susceptibility of soil to various types of internal erosion, including suffusion, contact erosion and backwards erosion, is governed by geometric and hydraulic conditions (Garner & Fannin 2010). The geometric criteria to judge base-filter compatibility is based on the particle size distribution (PSD) and assesses whether finer base particles can traverse the pore space of the coarser filter particles (Kenney & Lau 1985; Kézdi 1979). The hydraulic behavior determines the onset of internal erosion and

has been investigated through field-scale experiments. Terzaghi (1929) proposed an empirical equation to define the critical hydraulic gradient to initiate hydraulic heave failure:

$$i_{crit}=\frac{(1-n)\cdot(\gamma_s-\gamma_w)}{\gamma_w} \qquad \text{Equation 1}$$

where γ_w and γ_s are the specific weight of water and soil particles being uplifted respectively, and n is porosity. In the context of levees, Ojha, Singh and Adrian (2003) analyzed piping behaviors in different sand types, and proposed an empirical equation for the critical hydraulic gradient to initiate piping:

$$i_{crit}=\frac{4c}{\gamma_w}\left(1+\frac{\gamma_w^2 d_{50}^4}{512\mu^2 gL}\frac{c}{\gamma_w}\right) \qquad \text{Equation 2}$$

where L is the length of the levee perpendicular to the flow, μ is the dynamic viscosity of water, d_{50} is the median size of particles, g is gravitational acceleration and c is the coefficient of linear model of the critical shear stress $\tau_{crit}=cd_{50}$. Brauns (1985) tested layered soil specimens with different PSDs and found the critical flow velocity in the filter layer to trigger contact erosion to be:

$$u_{F,crit}=Fr_{crit}n_F\sqrt{\frac{(\gamma_{s,B}-\gamma_w)d_{50,B}}{\rho_w}} \qquad \text{Equation 2}$$

where properties of filter and base layer are denoted with the subscripts F and B respectively. The Froude number is defined as $Fr=\frac{u_{seep}}{\sqrt{gL_{char}}}$, where u_{seep} is the seepage flow velocity and L_{char} is the characteristic length. These empirical equations indicate that the critical hydraulic condition to trigger the onset of internal erosion is related to inherent physical properties of the seeping fluid (e.g. specific weight and viscosity) and field-scale soil properties (e.g. porosity and PSD).

However, the onset of internal erosion in field-scale experiments was only identified when material loss already occurred. This indicates that particle transportation has already been progressing, and thus the filed-scale onset point differs from that at the particle scale. Further, the hydraulic gradient or fluid flow velocity measurements in field-scale studies was conducted globally on the entire soil sample or filter layer, instead of locally within pores. The critical hydraulic condition inside a single pore to trigger the onset of particle-scale internal erosion, that is, the detachment of particles, is yet to be fully understood.

This study presents an experimental technique to quantitatively investigate particle-scale hydraulic influence on cohesionless base particle motion during the filtration erosion process. The apparatus and experimental procedure are explained in detail. The experimental process to measure the critical pore flow velocity that triggers filtration erosion is introduced in this paper. The intersecting influence of hydraulic conditions and geometric properties of soil assemblies can be studied with this apparatus. The investigation on particle-scale fluid behaviors in filtration erosion can give new insight into material's susceptibility to filtration erosion, as well as hydraulic behaviors to

trigger the onset of filtration erosion.

METHODOLOGY

Experimental apparatus

The apparatus used for this technique is schematically illustrated in Figure 1 and comprised three core components: (1) seepage cell containing sphere packing; (2) water circulation system; and (3) imaging system. These three components are discussed in detail below.

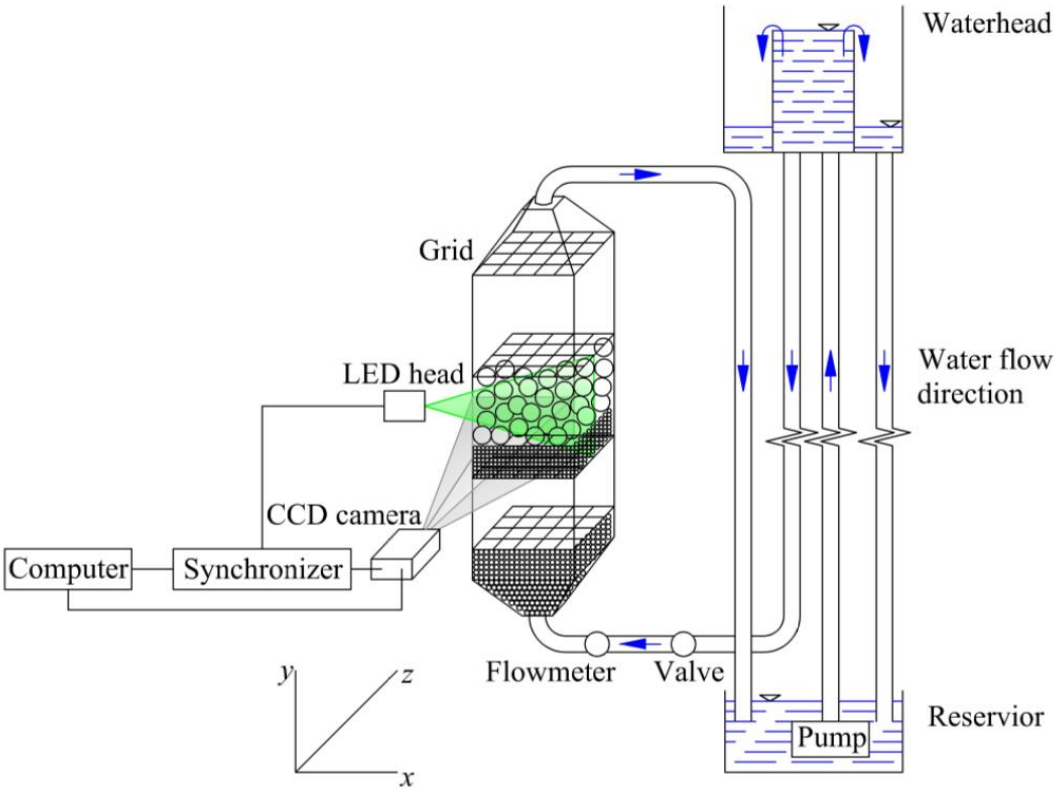

Figure 1 Experimental apparatus

1. Seepage cell

The seepage cell contains the sphere packing for simulating the base-filter combination in filtration erosion. The seepage cell is a 10 cm × 10 cm × 30 cm (W × L × H) square hollow Plexiglas column with full optical access. Two conical funnel openings were placed at both ends of the seepage cell, and were connected to the rest of the water circulation system with pipes.

The filtration erosion process was investigated in an idealized manner by considering two layers of monodisperse spheres of different sizes representing the filter and the base particle layers. Preliminary studies considered 2-mm-diameter glass

spheres for base particles, and 12-mm-diameter hydro-gel spheres for filter particles. More complex PSD combinations will be applied with this experimental setup in future studies. The entire sphere packing was assembled dry and without compaction. All glass spheres were poured into the seepage cell at one time to form the base layer. Hydro-gel spheres were soaked in tap water for at least four hours until fully hydrated and swelled. Fully hydrated hydro-gel spheres were then drained and poured on top of base particles by layers as filter particles, with care to prevent mixture of base and filter particles at this stage.

Error! Reference source not found. illustrates a force analysis of a cohesionless particle in a fluid flow field. The force *G'* is the net force due to gravity, *G*, and buoyancy, *B*:

$$G'=G-B=(\gamma_s-\gamma_w)\cdot V \qquad \text{Equation 3}$$

where *V* is the particle volume. *G'* relates only to the inherent property of the particle and the fluid. The interaction force, F_{fluid}, is the net force imparted by the fluid on the particle and comprises contribution due to pressure gradient, F_p, and drag force, F_d (Falkovich 2011):

$$F_{fluid}=F_p-F_d=V\cdot\nabla_p+CR^2\rho_w u^2 \qquad \text{Equation 4}$$

where *C* is a dimensionless drag coefficient, *R* is the spherical radius, and *u* is the relative velocity between fluid and sphere. When the fluid flow velocity is sufficiently large, the driving force F_{fluid} will exceed the resisting forces on the particles, resulting in detachment and motion of the base particles. The fluid flow velocity at which the driving force exceeds the resisting force of base particles was the focus of this study, and is referred to as the critical flow velocity in the following discussion.

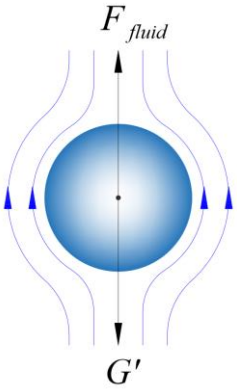

Figure 2 Force analysis for cohesionless sphere in fluid flow

According to Equation 4 and 5, the critical flow velocity is high for base particles with high specific weight in relation to the fluid. Therefore, base particle material with a reasonably high specific weight ensures the critical flow velocity measurement to be feasible, without causing fluidization at lower flow velocity. The specific weight of glass beads was approximately 2.5 times of water, and was suitable as base particle material. In addition, the glass surface was smooth, and can simulate the cohesionless contact

between base particles. Thus, glass spheres were ideal material for simulating the cohesionless base particles to gain fundamental insights into the initiation of filtration erosion.

The crucial requirement for filter particles was to be transparent in the liquid-phase material. This implied that the filter particle material needed to be refractive index matched (RIM) with the fluid. This allowed the pore space within the filter particles to be optically accessible to measure pore flow velocity. Hydro-gel was an ideal material to achieve RIM with water (Byron & Variano 2013; Lo et al. 2009; Weitzman et al. 2014), due to its high volumetric water content of up to 99% when fully hydrated (Lo et al. 2009). This characteristic made hydro-gel spheres suitable for simulating filter soil particles for PIV observation.

However, hydro-gel spheres had similar density to water and were highly compressible. Hydro-gel sphere skeletons can be easily disturbed by fluid flow, which may result in bias to measurements. One possible solution is to replace the hydro-gel spheres with glass spheres of the same size. Fluid in this system then needs to be modified to attain RIM with glass. Tuned aqueous solutions or organic liquids are required. The proportion of different compositions of the liquid mixtures must be precisely manipulated (Budwig 1994; Wiederseiner et al. 2011). The liquid components must be non-toxic, safe to work with and not dissolve or react with components of the experimental apparatus (Budwig 1994). In addition, the refractive indices are affected by external factors including temperature and humidity (Wiederseiner et al. 2011). Therefore, the RIM liquid mixtures must be carefully stored to maintain the physical properties.

2. Water circulation system

The fluid needed to be seeded with tracers to visualize fluid motion using the PIV system. Tracers must have the same density as the fluid (Melling 1997) with small volume to accurately capture the flow. Tracers must also be reflective to be observed through the PIV camera (Raffel et al. 1998). In this study, 20-μm-diameter Polyamide Seeding Particles (PSPs) manufactured by Dantec Dynamics A/S were used as tracers, and were seeded into water before commencement of experiments at a volume concentration of 0.1%. Due to the relatively small size compared to the pore throats, the tracers have minimal influence on the flow field.

To configure the PSP-seeded water to circulate in this system, a water circulation system was implemented. Blue arrows in Figure 1 indicate the flow direction. The upwards seepage flow to induce filtration erosion in the seepage cell was enabled by a constant pressure water head, which was functioned with a double-layer cylinder. Water was pumped from the reservoir through a pipe into the inner cylinder. As water was being constantly pumped into the inner cylinder, excess water outflowed into the outer cylinder, and the water surface of the inner cylinder remained constant. Water in the outer cylinder was directed back into the reservoir. The bottom of the inner cylinder was connected to the bottom of seepage cell to provide the upward seepage water flow. The flow rate can be adjusted with a valve and measured with a flowmeter. After travelling

through the seepage cell, water overflowed from the top of the seepage cell, and was directed back to the reservoir. PSP-seeded water then circulated within the system.

Pipe flow experiencing sudden expansions in cross-sectional area is subjected to the influence of expansion effect. The expansion effect causes disturbance, which leads to vortices and backwards (against the flow-wise direction) streamlines in flow regimes (Drikakis 1997). The disturbance brought a non-uniform fluid boundary condition to the sphere packing inside the seepage cell. To mitigate the disturbance, a pebble bed was placed in the bottom funnel opening of the seepage cell. In preliminary tests, pebble beds formed with different sizes of glass spheres were placed in the bottom opening to observe how flow regimes in an empty seepage cell were influenced. The results showed that the pebble bed formed with 5-mm-diameter glass spheres was suitable for filtration erosion tests. Its permeability allowed the required flow rate range to be attained. Meanwhile, uniform and upwards flow was observed at this flow rate range. Besides placing the pebble bed, the sphere packing was then fixed in the middle part of the seepage cell, where water flow was observed to be most uniform.

3. Particle image velocimetry (PIV) system

The PIV technique is widely adopted for measuring micro-scale velocity field (Adrian 1986; Santiago et al. 1998; White, Take & Bolton 2003). The PIV system applied in the current study consisted of a high-speed charge-coupled device (CCD) camera, a pulsed light-emitting diode (LED) head as the light source, a synchronizer to control the working time pace of the camera and light source, and a computer to operate the system. The focal axis of the CCD camera was set perpendicular to the light sheet generated by the LED head. By moving the LED head along the z-axis, different cross-sections in the sphere packing were illuminated and observed. Meanwhile, by moving the camera around the xy-plane, images of different areas can be acquired.

The CCD camera acquired consecutive images in the studied area. The time interval between two exposures was user-defined. The pulsed illumination functioned at the same pace as the camera. The reflective PSP tracers seeded in the fluid were illuminated by the light source and could be observed through the camera as shown in Figure 3 (a). By measuring the displacement of each tracer particles between two consecutive images, the velocity vector was calculated with the known time interval between the two exposures (Raffel et al. 1998).

The time interval between two exposures needed to be calibrated with the flow velocity to ensure that valid and appropriate displacements took place in the fluid flow field between two exposures (Fischer, Sauvage & Roehle 2008; Gori, Petracci & Angelino 2013). A longer time interval was required for lower pore flow velocity to ensure that detectable displacements took place. A shorter time interval was required for higher pore flow velocity to ensure that the detected tracer particles did not exceed the detection area in the following image. Preliminary tests were conducted to find appropriate time interval for the flow rate range applied in the filtration tests. Different time intervals were attempted to avoid invalid vectors in image processing. The time interval range used in this study was between 20 μs and 50 μs for superficial flow

velocity between 0.013 m/s and 0.025 m/s.

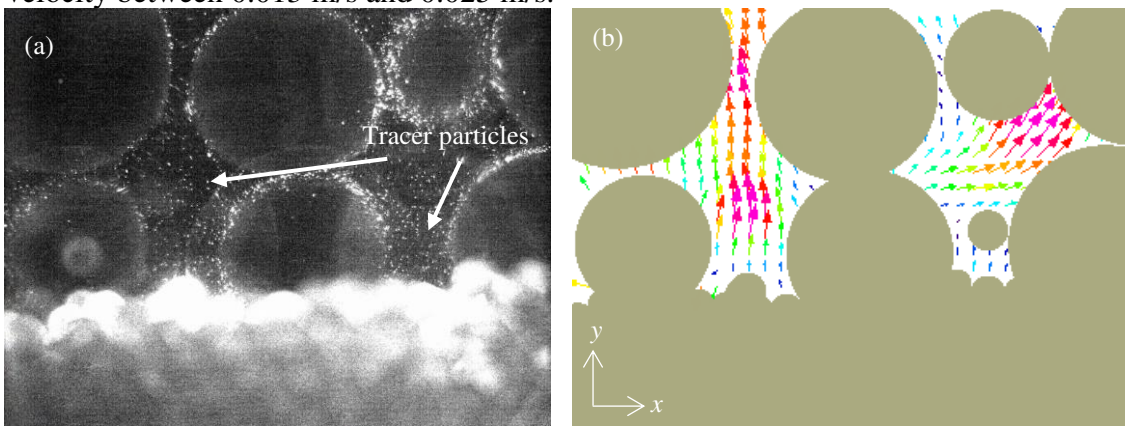

Figure 3 (a) PIV view at the filter/base interface; (b) PIV analysis result when a base particle detaches

The PIVview 2C software developed by PIVTEC GmbH was used for image processing in this study. The software divided the acquired images into numerous small interrogation windows (IWs). The velocity vector for each detected tracer particle in an IW was calculated. The mean velocity vector of all detected tracer particles within an IW was defined as the overall velocity vector for this IW. All IW velocity vectors within the observed frame of view (FOV) assembled the entire velocity vector field (Raffel et al. 1998). Figure 3 (b) shows an example of the velocity vector field generated with PIVview 2C.

However, the current experimental setup was restricted to acquire images and consequently velocity fields in a two-dimensional *xy*-plane. The velocity component along the *z*-axis was not captured. In pores that are aligned along the *z*-axis, that is, perpendicular to the image plane, the *z*-component of pore flow velocity cannot be ignored. Therefore, a stereoscopic PIV system with additional CCD cameras is suggested to detect the three-component velocity vector field for such spatial pores. Prasad and Adrian (1993) proposed a stereoscopic PIV technique that can be easily adopted by the current experimental setup.

Experimental procedure

Experiments were conducted with this technique to measure the critical pore flow velocity to trigger filtration erosion. Figure 5 shows a schematic view at the base-filter interface. A velocity vector field for pore flow in the hydro-gel sphere matrix was obtained with the PIV technique. The pore flow velocity was defined as the mean velocity along the pore throat, i.e. where the distance between two filter particles was the shortest. The starting point of filtration erosion was recognized when a base particle started to detach into the intruded pore. Pore flow velocity at the starting point was considered to be the quantitative measurement for filtration erosion initiation.

To trigger the filtration erosion process, the valve was adjusted to slowly increase

the seepage flow rate in the seepage cell. Once a base particle in the observed area started to detach, the flow rate was kept constant. The camera recorded the whole process of increasing flow rate, and the frame when a base particle detached was taken for image analysis. By moving the LED head and the CCD camera, the flow behaviors at different

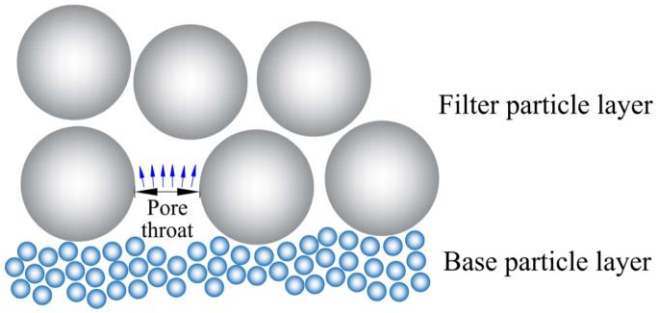

Figure 4 Schematic representation of the filter/base interface

cross-sections of the seepage cell could be observed.

SUMMARY AND RECOMMENDATION

This paper presents an experimental technique to study particle-scale fluid behaviors in filtration erosion. Two layers of spherical particles of different sizes were used to form the filter-base sphere packing for simulating filtration erosion. The filtration erosion process was driven by an external upwards seepage flow. A particle-scale flow velocity vector field in the pore space of the filter particles was obtained with a PIV system. The critical pore flow velocity to trigger base particles' detachment could be measured with this technique.

Modifications can be made to the system for other studies concerning filtration erosion, including:

- Geometric factors' influence on filtration erosion behaviors can be investigated by modifying the sphere packing. For example, the shape, particle size distribution, or volume fraction of the sphere packing can be modified.
- Other types of internal erosion can be studied by modifying the arrangement of the base/filter combination. For example, suffusion can be investigated by inserting base particles into the filter layer.

The following are recommended to improve the current experimental setup:

- Hydro-gel spheres that simulate filter particles can be replaced with glass spheres. A RIM liquid is then required. The liquid needs to be carefully tuned and stored to maintain the physical properties.
- The current PIV system can be modified into stereoscopic by adding an additional camera. A stereoscopic system can obtain three-component velocity information in the illuminated plane. It is suitable for measuring pore flow velocity in spatial pores.

REFERENCES

Adrian, R 1986, 'Image shifting technique to resolve directional ambiguity in double-pulsed velocimetry', *Applied Optics*, vol. 25, no. 21, pp. 3855-8.

Brauns, J 1985, 'Erosionsverhalten gechichteten Bodens bei horizontaler Durchströmung', *Wasserwirtschaft*, vol. 75, no. 10, pp. 448-53.

Budwig, R 1994, 'Refractive index matching methods for liquid flow investigations', *Experiments in fluids*, vol. 17, no. 5, pp. 350-5.

Byron, ML & Variano, EA 2013, 'Refractive-index-matched hydrogel materials for measuring flow-structure interactions', *Experiments in fluids*, vol. 54, no. 2, p. 1456.

Drikakis, D 1997, 'Bifurcation phenomena in incompressible sudden expansion flows', *Physics of Fluids*, vol. 9, no. 1, pp. 76-87.

Falkovich, G 2011, *Fluid Mechanics: A Short Course for Physicists*, Cambridge University Press, Cambridge.

Fischer, A, Sauvage, E & Roehle, I 2008, 'Acoustic PIV: Measurement of the acoustic particle velocity using synchronized PIV-technique', *Journal of the Acoustical Society of America*, vol. 123, no. 5, p. 3130.

Garner, S & Fannin, R 2010, 'Understanding internal erosion: a decade of research following a sinkhole event', *The International Journal on Hydropower Dams*, vol. 17, no. 3, p. 93.

Gori, F, Petracci, I & Angelino, M 2013, 'Flow evolution of a turbulent submerged two-dimensional rectangular free jet of air. Average Particle Image Velocimetry (PIV) visualizations and measurements', *International Journal of Heat Fluid Flow*, vol. 44, pp. 764-75.

Kenney, T & Lau, D 1985, 'Internal stability of granular filters', *Canadian Geotechnical Journal*, vol. 22, no. 2, pp. 215-25.

Kézdi, Á 1979, *Soil physics: selected topics*, vol. 25, Elsevier, Amsterdam.

Li, M & Fannin, RJ 2008, 'Comparison of two criteria for internal stability of granular soil', *Canadian Geotechnical Journal*, vol. 45, no. 9, pp. 1303-9.

Lo, H-CJ, Tabe, K, Iskander, M & Yoon, S-H 2009, 'A transparent water-based polymer

for simulating multiphase flow', *Geotechnical Testing Journal*, vol. 33, no. 1, pp. 1-13.

Melling, A 1997, 'Tracer particles and seeding for particle image velocimetry', *Measurement Science Technology*, vol. 8, no. 12, p. 1406.

Ojha, C, Singh, V & Adrian, D 2003, 'Determination of critical head in soil piping', *Journal of Hydraulic Engineering*, vol. 129, no. 7, pp. 511-8.

Prasad, A & Adrian, R 1993, 'Stereoscopic particle image velocimetry applied to liquid flows', *Experiments in fluids*, vol. 15, no. 1, pp. 49-60.

Raffel, M, Willert, CE, Scarano, F, Kähler, CJ, Wereley, ST & Kompenhans, J 1998, *Particle image velocimetry: a practical guide*, Springer.

Reddi, LN, Ming, X, Hajra, MG & Lee, IM 2000, 'Permeability reduction of soil filters due to physical clogging', *Journal of Geotechnical and Geoenvironmental Engineering*, vol. 126, no. 3, pp. 236-46.

Santiago, JG, Wereley, ST, Meinhart, CD, Beebe, D & Adrian, R 1998, 'A particle image velocimetry system for microfluidics', *Experiments in fluids*, vol. 25, no. 4, pp. 316-9.

Terzaghi, K 1929, 'Effect of minor geologic details on the safety of dams', *Amer. Inst. Min. Met. Engrs. Tech. Publ.*, vol. 215, pp. 31-44.

Tomlinson, SS & Vaid, Y 2000, 'Seepage forces and confining pressure effects on piping erosion', *Canadian Geotechnical Journal*, vol. 37, no. 1, pp. 1-13.

Weitzman, JS, Samuel, LC, Craig, AE, Zeller, RB, Monismith, SG & Koseff, JR 2014, 'On the use of refractive-index-matched hydrogel for fluid velocity measurement within and around geometrically complex solid obstructions', *Experiments in fluids*, vol. 55, no. 12, p. 1862.

White, D, Take, W & Bolton, M 2003, 'Soil deformation measurement using particle image velocimetry (PIV) and photogrammetry', *Geotechnique*, vol. 53, no. 7, pp. 619-31.

Wiederseiner, S, Andreini, N, Epely-Chauvin, G & Ancey, C 2011, 'Refractive-index and density matching in concentrated particle suspensions: a review', *Experiments in fluids*, vol. 50, no. 5, pp. 1183-206.